

Article

Cometal Addition Effect on Superconducting Properties and Granular Behaviours of Polycrystalline FeSe_{0.5}Te_{0.5}

Manasa Manasa ¹, Mohammad Azam ¹, Tatiana Zajarniuk ², Ryszard Diduszko ^{2,3}, Tomasz Cetner ¹, Andrzej Morawski ¹, Andrzej Wiśniewski ² and Shiv J. Singh ^{1,*}

¹ Institute of High Pressure Physics (IHPP), Polish Academy of Sciences, Sokolowska 29/37, 01-142 Warsaw, Poland

² Institute of Physics, Polish Academy of Sciences, Aleja Lotników 32/46, 02-668 Warsaw, Poland

³ Institute of Microelectronics and Photonics, Wólczyńska 133, 01-919 Warsaw, Poland

* Correspondence: sjs@unipress.waw.pl

Abstract: The enhanced performance of superconducting FeSe_{0.5}Te_{0.5} materials with added micro-sized Pb and Sn particles is presented. A series of Pb- and Sn-added FeSe_{0.5}Te_{0.5} (FeSe_{0.5}Te_{0.5} + xPb + ySn; x = y = 0–0.1) bulks are fabricated by the solid-state reaction method and characterized through various measurements. A very small amount of Sn and Pb additions (x = y ≤ 0.02) enhance the transition temperature (T_c^{onset}) of pure FeSe_{0.5}Te_{0.5} by ~1 K, sharpening the superconducting transition and improving the metallic nature in the normal state, whereas larger metal additions (x = y ≥ 0.03) reduce T_c^{onset} by broadening the superconducting transition. Microstructural analysis and transport studies suggest that at x = y > 0.02, Pb and Sn additions enhance the impurity phases, reduce the coupling between grains, and suppress the superconducting percolation, leading to a broad transition. FeSe_{0.5}Te_{0.5} samples with 2 wt% of cometal additions show the best performance with their critical current density, J_c , and the pinning force, F_p , which might be attributable to providing effective flux pinning centres. Our study shows that the inclusion of a relatively small amount of Pb and Sn (x = y ≤ 0.02) works effectively for the enhancement of superconducting properties with an improvement of intergrain connections as well as better phase uniformity.

Keywords: iron-based high- T_c superconductors; critical transition temperature; critical current density; pinning force; transport and magnetic measurements



Citation: Manasa, M.; Azam, M.; Zajarniuk, T.; Diduszko, R.; Cetner, T.; Morawski, A.; Wiśniewski, A.; Singh, S.J. Cometal Addition Effect on Superconducting Properties and Granular Behaviours of Polycrystalline FeSe_{0.5}Te_{0.5}. *Materials* **2023**, *16*, 2892. <https://doi.org/10.3390/ma16072892>

Academic Editor: Daniele Torsello

Received: 7 March 2023

Revised: 1 April 2023

Accepted: 3 April 2023

Published: 5 April 2023



Copyright: © 2023 by the authors. Licensee MDPI, Basel, Switzerland. This article is an open access article distributed under the terms and conditions of the Creative Commons Attribution (CC BY) license (<https://creativecommons.org/licenses/by/4.0/>).

1. Introduction

Iron-based superconductors (FBSs) have attracted significant attention owing to their relatively high superconducting transition temperature (T_c) of 58 K [1–3]. In 2008, FBSs were discovered through F-doped LaOFeAs [3], and since then, more than 100 compounds have been reported belonging to this high- T_c superconductor. On the basis of parent compound structures, these compounds can be categorized into 6–7 families [2,4–6]: REOFeAs (1111) (RE = rare earth), AFe₂As₂ (A = Ba, K, Ca) (122), FeSe_xTe_{1-x} (11), CaKFe₄As₄ (1144), and LiFeAs (111), the 11 family. FeSe belongs to the 11 family [7,8] and has the simplest crystal structure [9,10] in FBSs. Generally, it shows a superconducting transition at 8 K which can be significantly enhanced up to 37.6 K under an applied external pressure of ~4.15 GPa [11]. Many new superconductors have been derived from FeSe with enhanced superconductivity, including A_xFe_{2-y}Se₂ (A = K, Rb, Tl, etc.) [12,13] and other organic intercalated superconductors, (Li, Fe)OHFeSe [14], heavily electron-doped FeSe through gating or potassium deposition, and in particular, single-layer FeSe/SrTiO₃ films with a record high T_c of ~100 K [15,16].

Various kinds of doping have been reported, such as Cu [17,18], Ni [19], Cr [20], Co [8] at Fe sites, and S [8,21,22] and Te [8] at Se sites, to understand the superconducting mechanism and to enhance superconducting properties [23]. It has been reported that when Te is substituted at Se sites, the highest T_c of up to 14.8 K is achieved with an optimal Te content of 50% [24]. Additionally, the 11 family does not contain any dangerous or rare

earth elements and shows a high critical density ($J_c \approx 8.6 \times 10^4$ A/cm² at 0 T, 2 K) and high upper critical field ($H_{c2} \approx 50$ T) [25,26] for single crystals, which is interesting for a range of applications, such as superconducting magnets, wires, and tapes [27]. On the other hand, preparing single-phase superconducting bulks is difficult for this 11 family because the complicated phase diagram of FeSe has many stable crystalline forms such as tetragonal β -Fe_xSe, hexagonal δ -Fe_xSe, orthorhombic FeSe₂, tetragonal β -Fe_xSe, monoclinic Fe₃Se₄, and hexagonal Fe₇Se₈, in which the tetragonal phase generally exhibits superconductivity with $T_c \sim 8$ K [7]. Some of these stable phases, particularly hexagonal δ -Fe_xSe and hexagonal Fe₇Se₈, appear with the main tetragonal β -Fe_xSe phase during the growth process and are not suitable for superconducting properties [28,29].

Several types of processes have been reported to enhance flux-pinning behaviours such as metal additions, chemical doping using different metallic and non-metallic phases, high-energy irradiation, and the admixing of nanoparticles [30]. Recent studies have shown that different metal additions may be an effective and feasible approach for enhancing the superconducting properties of FBSs by introducing additional pinning centres and comprehending the superconducting mechanism [2,6,30–33]. In high- T_c cuprate superconductors, the critical current density J_c of YBa₂Cu₃O_y (YBCO) is enhanced by Ag addition [34]. Ag or Pb addition to the 122 family (Sr_{0.6}K_{0.4}Fe₂As₂) also enhances J_c values with the improvement in grain connections. In a similar way, various kinds of metal additions, such as Ag [35], Co [36], Ni [36], Li [37], Pb [38], and Sn [39], are also reported for FeSe_{0.5}Te_{0.5} bulks to enhance superconducting properties. The reported studies suggest that the addition of Li, Pb, or Sn has a positive effect to improve either transition temperature T_c or critical current density J_c [37–39]. Therefore, further research works are needed to fully understand the impact of adding suitable metal elements and their appropriate weights to bulk superconductors to enhance all of their superconducting properties, i.e., T_c as well as J_c of FBSs at the same time with high-quality samples.

Chen et al. [39] studied 5 wt% ($x = 0, y = 0.05$) and 10 wt% ($x = 0, y = 0.10$) Sn-added FeSe_{0.5}Te_{0.5} samples, where the 5 wt% Sn-added samples improved the superconducting offset transition temperature (T_c^{offset}) significantly by ~ 3 K compared to that of Sn-free samples but had almost the same onset transition temperature (T_c^{onset}) value as that of the parent compound. However, there is no report for a small amount of Sn addition, such as less than 5 wt% ($y < 0.05$). Recently, Pb-added FeSe_{0.5}Te_{0.5} has also been studied, and these results indicate that the superconducting transition is decreased and the impurity phase is enhanced with Pb addition due to the reduced Fe/Se/Te ratio from the stoichiometric FeSe_{0.5}Te_{0.5} composition. However, 5 wt% Pb ($x = 0.05, y = 0$) addition has an onset T_c of 13.8 K and improves the J_c value in the measured magnetic field (up to 9 T) due to the improved grain connections. Hence, Pb addition weakens the superconducting transition of FeSe_{0.5}Te_{0.5} while enhancing the intergranular behaviour and the critical current properties for a sample with a small amount of Pb ($x = 0.05, y = 0$). These reported studies suggest that it would be worthwhile to conduct additional research on the optimisation of very low amounts of Pb and Sn addition, such as $x = y < 0.05$, and process parameters in order to improve superconductivity and critical current properties. However, there are no studies available based on cometal addition to FeSe_{0.5}Te_{0.5} polycrystalline samples or other families of iron-based superconductors. Because Pb effectively increases the critical current density [38] and Sn improves the quality of the superconducting transition as reported [39], it would be interesting to investigate the superconducting properties of FeSe_{0.5}Te_{0.5} with a small amount of both Pb and Sn addition, especially with a very low amount of additions. These are our main motivations behind this research paper.

In this study, we synthesised a series of low amounts of Pb- and Sn-added FeSe_{0.5}Te_{0.5} + x Pb + y Sn ($x = y = 0, 0.01, 0.02, 0.03, 0.04, 0.05$, and 0.10) and investigated the effects of Sn and Pb additions on the structure, microstructure, and superconducting properties of FeSe_{0.5}Te_{0.5} bulks. Structural and microstructural analysis shows that the impurity phases are increased with higher Pb and Sn additions $x = y \geq 0.03$; however, a low amount of addition such as $x = y \leq 0.02$ enhanced the superconducting transition by around 1 K and also improved the critical current

density. Our present study shows that a small amount of cometal addition is an effective way to improve grain connectivity, superconducting transition T_c , and pinning behaviours, resulting in an enhancement of the critical current density.

2. Experimental Details

The solid-state reaction method was used to grow the polycrystalline samples with nominal compositions of $\text{FeSe}_{0.5}\text{Te}_{0.5} + x\text{Pb} + y\text{Sn}$ ($x = y = 0, 0.01, 0.02, 0.03, 0.04,$ and 0.10). The initial steps involved mixing the starting materials, which were Fe powder (99.99% purity, Alfa Aesar, Ward Hill, MA, USA), Se (99.99% purity, Alfa Aesar), and Te (99.99% purity, Alfa Aesar), in accordance with the stoichiometric ratios of $\text{FeSe}_{0.5}\text{Te}_{0.5}$, for 15 min. More details about the synthesis process are reported elsewhere [38]. In the first step, the prepared pellets were sealed in an evacuated quartz tube which was heated to $600\text{ }^\circ\text{C}$ for 11 h in a box furnace. In the second stage, the prepared pellets were ground and mixed with 1 wt% ($x = y = 0.01$), 2 wt% ($x = y = 0.02$), 3 wt% ($x = y = 0.03$), 4 wt% ($x = y = 0.04$), 5 wt% ($x = y = 0.05$), and 10 wt% ($x = y = 0.1$) Pb and Sn (99% purity of Pb and Sn powder, respectively). These powders were pressed into pellets and sealed in an evacuated quartz tube, which was heated at $600\text{ }^\circ\text{C}$ for 4 h, followed by a furnace-cooling process. The final pellets had a diameter of 12 mm with a 2.5 mm thickness. To reduce oxygen and moisture during the synthesis, we performed all of the growth processes inside an inert gas glove box. Different batch samples were prepared to confirm the reproducibility of these bulk samples in terms of superconducting properties.

A structural analysis of all the prepared samples was examined using the powder X-ray diffraction method (XRD), which was performed on a Rigaku SmartLab 3 kW diffractometer with filtered $\text{Cu-K}\alpha$ radiation (wavelength: 1.5418 \AA , power: 30 mA, 40 kV), and a Dtex250 linear detector. The measuring profile was used from 5° to 70° with a very small step of $0.01^\circ/\text{min}$. The measured XRD data were analysed using the ICDD PDF4 + 2021 standard diffraction pattern database and Rigaku's PDXL software as well as Rietveld refinements using the Fullprof software [40] to perform the profile analysis, the quantitative values of impurity phases (%), and lattice parameter analysis for various samples. Microstructural characterisation was carried out using a field-emission scanning electron microscope. The magnetic measurements up to 9 T in the temperature range of 5–25 K under zero-field and field-cooling circumstances were carried out by Quantum Design PPMS using a vibrating sample magnetometer (VSM). During zero-field cooling (ZFC), the bulk sample was cooled down to 4 K, and then, after applying a magnetic field, the magnetic data were collected with increasing temperatures of 5 to 25 K. A closed-cycle refrigerator was used to measure the temperature dependence of the resistivity of rectangular-shaped samples in a zero magnetic field with various applied electric currents in a temperature range of 7 K to 300 K during the warming process.

3. Results and Discussion

Powder X-ray diffraction patterns of $\text{FeSe}_{0.5}\text{Te}_{0.5}$ with various amounts of Pb and Sn additions ($\text{FeSe}_{0.5}\text{Te}_{0.5} + x\text{Pb} + y\text{Sn}$) are depicted in Figure 1a. All samples showed the main tetragonal phase with space group $P4/nmm$. The parent compound ($x = y = 0$) also showed a small amount (~3–4%) of the hexagonal phase, which is similar to that of previously reported papers [38,39,41]. The diffracted peaks are not deviated by the additions of Pb and Sn, according to a comparison of the XRD patterns of the parent compound with Pb- and Sn-added samples, as shown in Figure 1a. It suggests that Pb and Sn do not enter into the tetragonal structure of $\text{FeSe}_{0.5}\text{Te}_{0.5}$. We also depicted the refined XRD patterns for low amounts of Pb- and Sn-added samples such as for $x = y = 0.01, 0.02,$ and 0.03 in Figure 1b–d, respectively. The obtained lattice parameters and the qualitative values of the impurity phases for various samples are listed in Table 1. The superconducting phase's crystallite size, as estimated by the XRD fitting data, was also mentioned in Table 1. The crystal size was greater for the sample with $x = y = 0.01$ and 0.02 than that of other samples, but as further Pb and Sn were added, the crystal size shrank.

Table 1. The obtained lattice parameters ‘a’ and ‘c’, the impurity phases, and the crystallite size of the main tetragonal phase for $\text{FeSe}_{0.5}\text{Te}_{0.5} + x\text{Pb} + y\text{Sn}$ samples are listed. We used Rigaku’s PDXL software and the ICDD PDF4 + 2021 standard diffraction patterns database for the quantitative analysis of impurity phases (%) and crystallite size through the refinement of the measured XRD data.

Sample	Lattice ‘a’ (Å)	Lattice ‘c’ (Å)	$\text{Pb}_{0.85}\text{Sn}_{0.15}\text{Te}_{0.85}\text{Se}_{0.15}$ (%)	Fe (%)	Hexagonal (%)	Crystallite Size (nm) ($\text{FeSe}_{0.5}\text{Te}_{0.5}$ Phase)
$x = y = 0$	3.7950	5.9713	-	-	3	34
$x = y = 0.01$	3.7977	5.9713	~2	-	<2	48.2
$x = y = 0.02$	3.7978	5.9665	~3	-	<2	46.0
$x = y = 0.03$	3.7958	5.9667	~6	-	-	42.1
$x = y = 0.04$	3.7995	5.9684	9	-	-	35
$x = y = 0.05$	3.7911	5.9639	14	-	-	33.5
$x = 0.05, y = 0$	3.7930	5.9611	-	-	-	45
$x = y = 0.1$	3.7921	5.9681	29	2	-	24.5

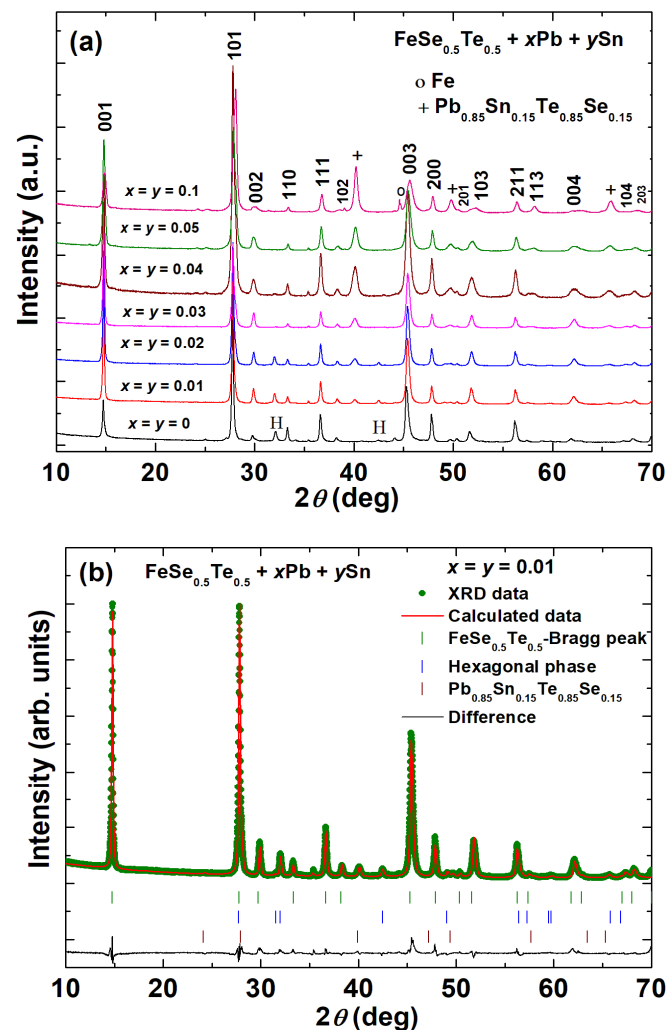


Figure 1. Cont.

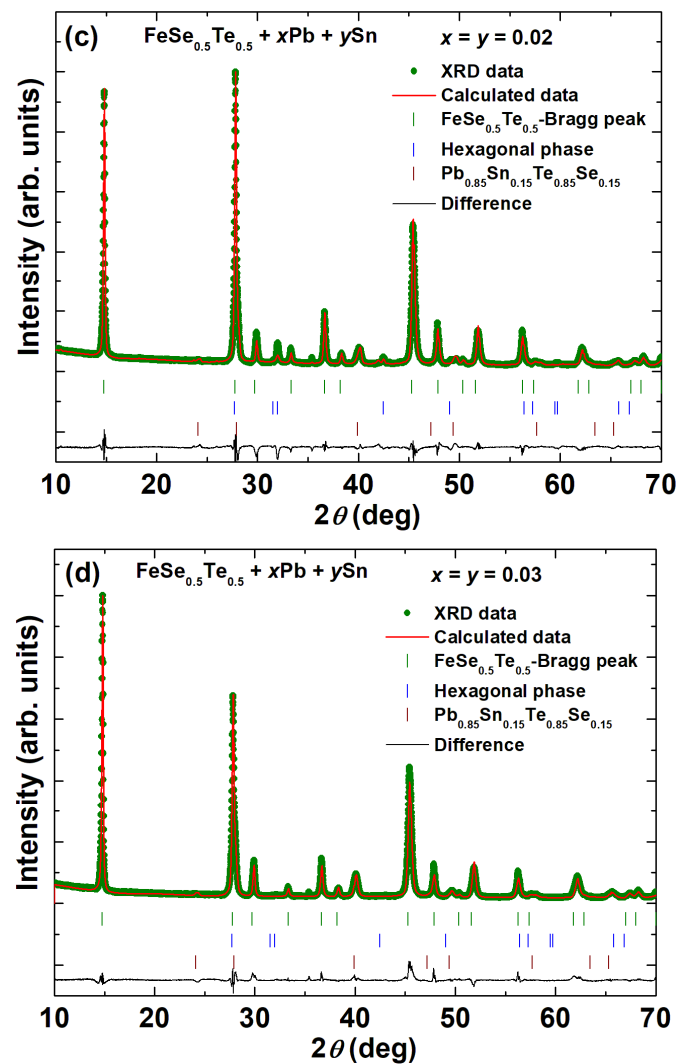


Figure 1. (a) X-ray diffraction patterns (XRD) of powdered FeSe_{0.5}Te_{0.5} + xPb + ySn ($x = 0, 0.01, 0.02, 0.03, 0.04, 0.05,$ and 0.1) samples. The fitted XRD patterns with the experimental, calculated diffraction patterns and their differences at room temperature are shown for the sample with (b) $x = y = 0.01,$ (c) $x = y = 0.02$ (d) $x = y = 0.03$. Instead of the nominal composition of FeSe_{0.5}Te_{0.5}, the tetragonal phase of Fe_{1.1}Se_{0.5}Te_{0.5} was observed as the real composition of the superconducting phase. One hexagonal phase, Fe₇Se₈, was left out in the refinement because of relatively weak reflections, whereas a hexagonal phase of Fe_{0.6}Se_{0.54}Te_{0.46} (~4–5%) was found and is depicted as ‘H’ in figure (a). The list of the obtained lattice parameters ‘a’ and ‘c’ and the obtained phases are listed in Table 1.

The parent compound has the lattice parameters ($a = 3.79502 \text{ \AA}, c = 5.9713 \text{ \AA}$) which are almost the same as the reported ones for bulk ($a = 3.7909 \text{ \AA}, c = 5.9571 \text{ \AA}$) and single crystals ($a = 3.815 \text{ \AA}, c = 6.069 \text{ \AA}$) of FeSe_{0.5}Te_{0.5} [8,41]. Interestingly, the hexagonal phase is notably reduced by a small amount of Pb and Sn addition ($x = y = 0.01$) and completely eliminated for $x = y = 0.03$ as depicted in Figure 1a–d, and this phase is not seen even at higher Pb and Sn additions similar to those reported for Pb [38] or Sn additions [39]. However, for Pb- and Sn-added samples, the Pb_{0.85}Sn_{0.15}Te_{0.85}Se_{0.15} phase appeared as an impurity phase which is very tiny for $x = y = 0.01$ and 0.02 but increases in intensity with further increase in Pb and Sn additions. Impurity phase enhancement is very similar to that of Sn- or Pb-added FeSe_{0.5}Te_{0.5} [38,39]. In the case of Sn-added FeSe_{0.5}Te_{0.5} [39], SnSe_{0.3}Te_{0.7}, and Fe₃O₄ exist in the Sn-added samples, and their intensities increase as the amount of Sn addition increases. In higher Pb addition to bulk FeSe_{0.5}Te_{0.5} [38], three extra phases such as PbTe, FeSe_{1-δ}, and Fe appeared as the impurity phases in which PbTe was observed as a dominant impurity

phase, suggesting a lower Te content in the $\text{FeSe}_{0.5}\text{Te}_{0.5}$ composition. The existence of the $\text{Pb}_{0.85}\text{Sn}_{0.15}\text{Te}_{0.85}\text{Se}_{0.15}$ phase in this present study suggests a reduced concentration of Se/Te in the $\text{FeSe}_{0.5}\text{Te}_{0.5}$ composition. At high amounts of Pb and Sn additions, we also observed a small amount of Fe as an impurity phase, as mentioned in Table 1. The obtained lattice parameters for various samples, seen in Table 1, indicate divergence with cometal additions with respect to the parent compound ($x = y = 0$), which suggests slightly lower Te/Fe/Se contents. Due to the presence of the various impurity phases, the refinement error is slightly higher for large amounts of Sn and Pb additions. It is important to note that excessive Sn and Pb additions can decrease the Fe/Te/Se concentrations in $\text{FeSe}_{0.5}\text{Te}_{0.5}$ compositions, whereas moderate levels of these additions can promote the formation of a tetragonal superconducting phase, similar to what has been observed in Pb or Sn-added $\text{FeSe}_{0.5}\text{Te}_{0.5}$ [38,39].

These polycrystalline samples with $x = y = 0, 0.01, 0.02, 0.03, 0.04, 0.05,$ and 0.1 were also subjected to an elemental analysis using the energy dispersive X-ray (EDAX) method, which allows for the measurement of the actual composition of the elements, as listed in Table 2. The homogenous distribution of the constituent elements is observed for $x = y = 0$ and $0.01, 0.02,$ and 0.03 , as confirmed by results in Table 2. However, because of the impurity phase, the distribution of Sn and Pb in the samples with $x = y \geq 0.04$ is not uniform, and some regions were found to be rich in Pb, Sn, Se, and Te, which proposes the existence of an impurity phase of $\text{Pb}_{0.85}\text{Sn}_{0.15}\text{Te}_{0.85}\text{Se}_{0.15}$, consistent with XRD results. The parent compound shows a molar ratio of 1:0.49:0.51 which is almost the same as the low amount of cometal additions. However, with a high amount of Pb and Sn additions, deviation with this molar ratio and the actual weight percent of cometal increases. These findings suggest that excessive additions of Sn and Pb result in non-uniform element distributions.

Table 2. List of molar ratios of various elements presented in $\text{FeSe}_{0.5}\text{Te}_{0.5} + x\text{Pb} + y\text{Sn}$ bulks.

Sample	Fe Molar Ratio	Te Molar Ratio	Se Molar Ratio	Pb (%)	Sn (%)
$x = y = 0$	1	0.49	0.5	-	-
$x = y = 0.01$	1	0.5	0.49	0.98	0.99
$x = y = 0.02$	1	0.5	0.5	1.5	2
$x = y = 0.03$	1	0.52	0.48	2.4	2.6
$x = y = 0.04$	1	0.53	0.42	3.16	4.1
$x = y = 0.05$	1	0.51	0.58	3.7	5.1
$x = 0.05, y = 0$	1	0.51	0.49	-	-
$x = y = 0.1$	0.98	0.47	0.57	4.5	7.98

To perform the microstructural analysis, we polished the pellet samples by using micron paper inside the glove box and collected backscattered scanning electron microscopy (BSE-SEM, revealing chemical contrast) images at different magnifications for different Sn- and Pb-added samples. Figure 2 shows BSE images for $x = y = 0, 0.02, 0.03,$ and 0.1 from low- to high-magnification images, respectively. We have observed three contrasts in our samples: light grey, white, and black contrasts corresponding to the phases of $\text{FeSe}_{0.5}\text{Te}_{0.5}$, $\text{Pb}_{0.85}\text{Sn}_{0.15}\text{Te}_{0.85}\text{Se}_{0.15}$, and pores, respectively. The parent compound has light grey and black contrasts that are observed as almost homogeneous in microstructure images on the microscale, as depicted in Figure 2a–c. Furthermore, these images also confirm that the samples with $x = y = 0$ have many well-connected and disk-shaped grains with an average size of $\sim 1\text{--}3 \mu\text{m}$, and in some places, micropores are also observed. A minor amount of Sn and Pb addition ($x = y = 0.01, 0.02$) slightly increased the grain size ($\sim 3\text{--}4 \mu\text{m}$) while decreasing pore sizes (from micro- to nano-range). Hence, many nanopores are observed, which results from the improved grain connectivity and sample density due to the reduced pore size compared to the parent compound, as shown in Figure 2d–f. Furthermore, regarding the phase of $\text{Pb}_{0.85}\text{Sn}_{0.15}\text{Te}_{0.85}\text{Se}_{0.15}$, we saw a few brighter contrasts in the sample (Figure 2d–f), similar to XRD analysis.

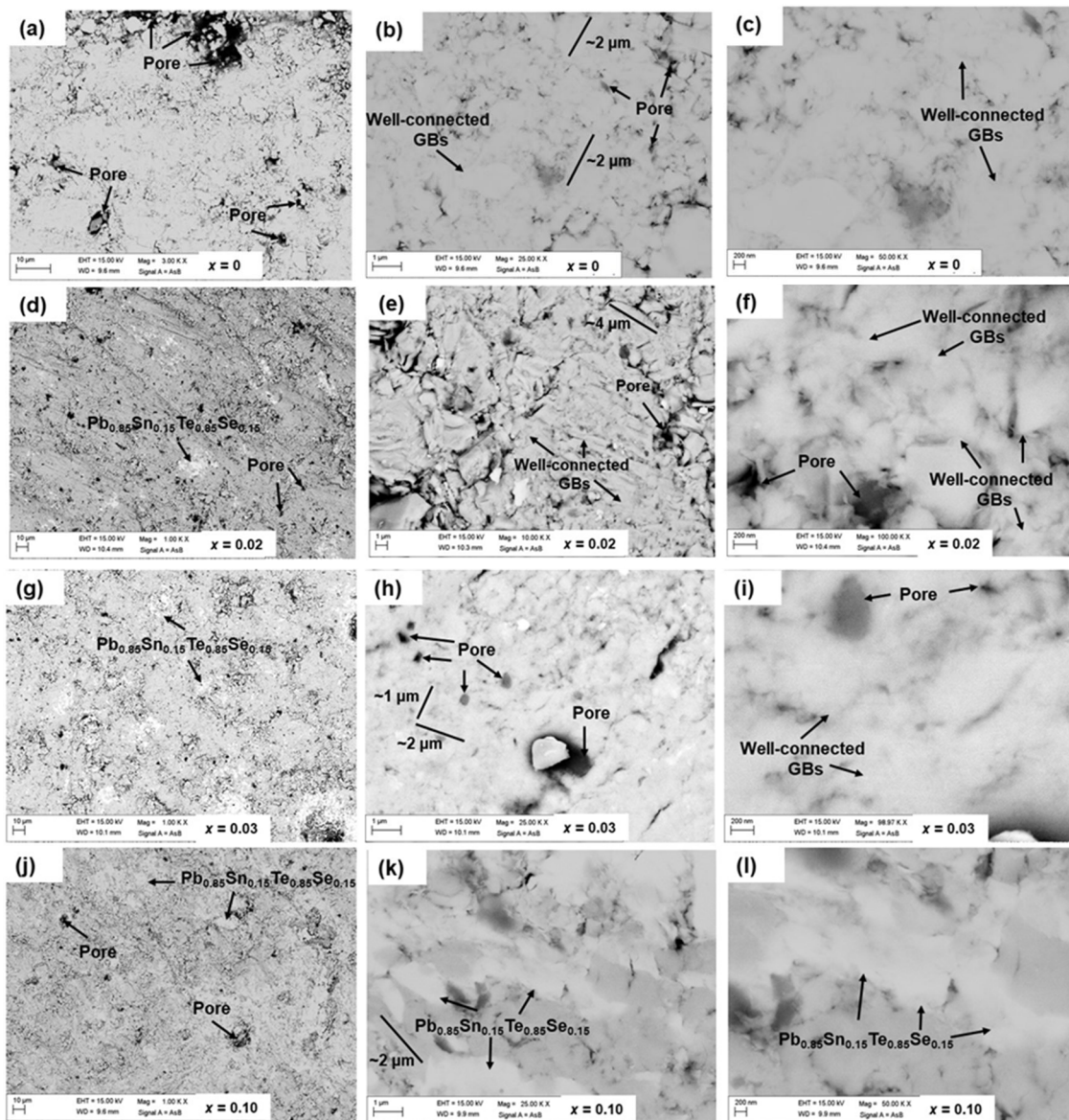


Figure 2. Back-scattered (BSE) images of various Pb and Sn-added $\text{FeSe}_{0.5}\text{Te}_{0.5} + x\text{Pb} + y\text{Sn}$ polycrystalline samples: (a–c) for $x = y = 0$; (d–f) for $x = y = 0.02$; (g–i) for $x = y = 0.03$ and (j–l) for $x = y = 0.10$. Bright contrast, light grey, and black contrast correspond to the phase of $\text{Pb}_{0.85}\text{Sn}_{0.15}\text{Te}_{0.85}\text{Se}_{0.15}$, $\text{Fe}(\text{Se}, \text{Te})$ and pores, respectively. The approximate grain size is depicted by the solid line.

With further increasing the Pb and Sn additions, the improvement in the microstructure was observed with the enhancement of the brighter phase with respect to $\text{Pb}_{0.85}\text{Sn}_{0.15}\text{Te}_{0.85}\text{Se}_{0.15}$, as shown in Figure 2d–f. It seems that the $\text{Pb}_{0.85}\text{Sn}_{0.15}\text{Te}_{0.85}\text{Se}_{0.15}$ phase filled up many nanopores, so we observed comparatively fewer nanopores for $x = y = 0.02$ compared to the bulk samples with $x = y = 0.01$ but almost the same grain size of $\sim 3\text{--}4\ \mu\text{m}$. Hence, it suggests further improvement in grain connectivity and the density of materials. Figure 2g–i show BSE images for $x = y = 0.03$ where the most prominent phase of $\text{Pb}_{0.85}\text{Sn}_{0.15}\text{Te}_{0.85}\text{Se}_{0.15}$ is observed as a white contrast randomly in the bulk sample at many places, i.e., inside grains and at grain boundaries, and also the size of pores as a black contrast is increased compared to samples with low Pb and Sn additions ($x = y \leq 0.02$). The existence of pores and impurity phases in the sample results in weak grain connections, and the plate-shaped grains are observed with an average grain size of $\sim 1\text{--}2\ \mu\text{m}$, as observed from Figure 2g–i. For further cometal additions ($x = y > 0.03$), a white contrast ($\text{Pb}_{0.85}\text{Sn}_{0.15}\text{Te}_{0.85}\text{Se}_{0.15}$) is observed in larger areas and at many regions of the sample,

and the reduced grain size is also observed as depicted in Figure 2j–l for $x = y = 0.1$. The increased impurity phase ($\text{Pb}_{0.85}\text{Sn}_{0.15}\text{Te}_{0.85}\text{Se}_{0.15}$) that is sandwiched between $\text{FeSe}_{0.5}\text{Te}_{0.5}$ grains often considerably reduces grain-to-grain connections and creates a strong barrier to intergranular supercurrent routes. It is well known from other iron-based superconductors that substantial cracking occasionally occurs at grain boundaries and within grains, but we did not see any micro-cracks between the grains in any of our bulk samples [42,43]. Since $\text{FeSe}_{0.5}\text{Te}_{0.5}$ has a theoretical density of 6.99 g/cm^3 [7,44], on this basis, we calculated the sample density by assuming the pure phase of $\text{FeSe}_{0.5}\text{Te}_{0.5}$ for our various samples, which are obtained around 51%, 61.9%, 65.6%, and 50.8%, for $x = y = 0, 0.01, 0.02$, and 0.03 , respectively. It indicates that a very small amount of Sn and Pb content added to the parent sample slightly enhanced the sample density as also observed from the microstructure analysis. Analysis of Figure 2 clearly demonstrates that a very small amount of Pb and Sn addition ($x = y \leq 0.02$) improves grain connectivity and sample density and decreases pores in contrast to a larger amount of Pb and Sn additions ($x = y > 0.02$), which reduce the phase purity and cleanness of grain boundaries and increases the number of pores. Non-superconducting phases at the grain boundaries of $\text{FeSe}_{0.5}\text{Te}_{0.5}$ for higher cometal additions generally create a problem for superconducting properties, as also reported for Pb-added Sr122 [45], Pb-added $\text{FeSe}_{0.5}\text{Te}_{0.5}$ [38], and Sn-added $\text{FeSe}_{0.5}\text{Te}_{0.5}$ [39]. As a result, our analysis suggests that a very small amount of Pb and Sn additions work effectively to increase material density while also improving grain size and connectivity.

Figure 3 depicts the DC magnetic susceptibility ($\chi = 4\pi M/H$) in both zero-field-cooled (ZFC) and field-cooled (FC) magnetisation curves for samples, $x = y = 0$ and $x = 0.05, y = 0$; $x = y = 0.01, x = y = 0.02$ and $x = y = 0.03$ measured under an applied magnetic field of 20 Oe in the temperature range of 5–20 K. We have shown the normalised magnetic susceptibility for all these samples for a comparison point of view. What one can safely conclude from Figure 3 is that the studied samples are bulk superconductors. Superconducting transition is observed at 14 K with a sharp diamagnetic transition in the magnetic susceptibility (χ) in both the ZFC and FC situations for the parent compound ($x = y = 0$). Only the Pb-added sample ($x = 0.05, y = 0$) shows the onset transition at 13.3 K and has a broader transition than that of the parent compound. Interestingly, a small amount of Pb and Sn such as $x = y = 0.01$ slightly enhanced the transition temperature ($T_c \sim 14.8$ K) with the sharpness of transition compared to the sample $x = 0.05, y = 0$. With the further addition of Pb and Sn, almost the same superconducting onset transition of 14.7 K is observed for $x = y = 0.02$ with better sharpness of the transition compared to other samples. However, a further increase in Pb and Sn additions reduces the transition temperature with the large broadening of the transition. It might be possible due to the formation of impurity phase $\text{Pb}_{0.85}\text{Sn}_{0.15}\text{Te}_{0.85}\text{Se}_{0.15}$ and to reduce the actual content of Te and Se from the main phase $\text{FeSe}_{0.5}\text{Te}_{0.5}$ as discussed above with the XRD data and the microstructural analysis. The single-step transition of each sample can be explained by the intergranular properties of these bulk samples, as discussed and reported for other FBS families [46]. These analyses also confirm that a very low amount of Sn- and Pb-added samples ($x = y \leq 0.02$) are effective for the superconducting properties of $\text{FeSe}_{0.5}\text{Te}_{0.5}$ similar to the conclusion of microstructural analysis and XRD measurements. Further, T_c is decreased as Sn and Pb concentrations are increased, possibly due to changes in Te/Se concentrations.

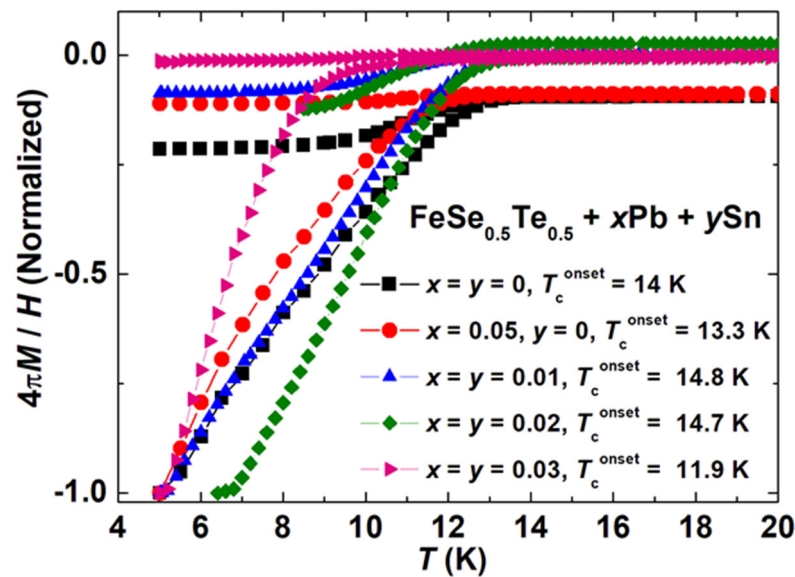


Figure 3. The variation of magnetic susceptibility ($\chi = 4\pi M/H$) with temperature for various $\text{FeSe}_{0.5}\text{Te}_{0.5} + x\text{Pb} + y\text{Sn}$ ($x = y = 0, 0.01, 0.02, 0.03$, and also $x = 0.05, y = 0$) bulks at the applied magnetic field of 20 Oe under zero-field-cooled (ZFC) and field-cooled (FC) regimes.

The temperature dependence of the resistivity (ρ) is shown in Figure 4a–c for the nominal compositions of polycrystalline $\text{FeSe}_{0.5}\text{Te}_{0.5} + x\text{Pb} + y\text{Sn}$ ($x = y = 0–0.1$) in a zero magnetic field. Due to the structural phase transition, the parent $\text{FeSe}_{0.5}\text{Te}_{0.5}$ ($x = y = 0$) exhibits a large anomaly in resistivity at a temperature of below ~ 110 K [47]. As reported [38] for Pb-added Fe(Se, Te), the electrical behaviour of this sample gradually changed, and a somewhat higher value of the normal state resistivity was observed due to the tiny amount and uneven distribution of the impurity PbTe phase with only Pb addition ($x = 0.05, y = 0$), and this resistivity anomaly also appeared for these Pb-added samples ($x = 0.05, y = 0$). A small amount of Sn and Pb addition to $\text{FeSe}_{0.5}\text{Te}_{0.5}$ up to $x = y = 0.03$ increases the metallic behaviour and its resistivity decreases in the whole temperature range. Interestingly, the anomaly related to the structural phase transition is also observed for these samples. A kink or concavity feature appeared for samples with very low amounts of Pb and Sn ($x = y = 0.01, 0.02$ and 0.03) below 80 K, which is similar to the behaviour reported for FeSe [48] or Fe(Se, Te) samples [49], and is usually linked with the weak structural distortion or attributed to the weak localisation effect [48,49].

With further enhancements of Pb and Sn additions ($x = y \geq 0.03$), the resistivity started to increase in the normal state and showed semi-metallic behaviour below the structural phase transition. The amount of the $\text{Pb}_{0.85}\text{Sn}_{0.15}\text{Te}_{0.85}\text{Se}_{0.15}$ phase is enhanced very rapidly for samples with $x = y > 0.03$ as discussed above, and its distribution inside the sample became more homogeneous with a reduction in the whole sample density as observed from the microstructural analysis, which could be a reason for the enhancement of the normal state resistivity, as in Figure 4a, which is visible more clearly below the structural transition. The sample with $x = y = 0.1$ has shown high resistivity values within the whole measured temperature range due to the very large amount of impurity phases. However, the low amount of addition of Pb and Sn ($x = y \leq 0.02$) increased the density of the samples, as discussed in the microstructural analysis, which could be a reason for the decreased resistivity of these samples and supported the formation of the superconducting tetragonal phase. The observed properties of the sample with $x = y = 0.03$ depict the combined effect of low and high amounts of Pb and Sn additions, suggesting that this could be the optimum cometal addition level. Due to the presence of impurity phases, the higher Sn- and Pb-added samples ($x = y > 0.02$) had a negative slope of resistivity below 120 K, which primarily manifests as semi-metallic behaviour.

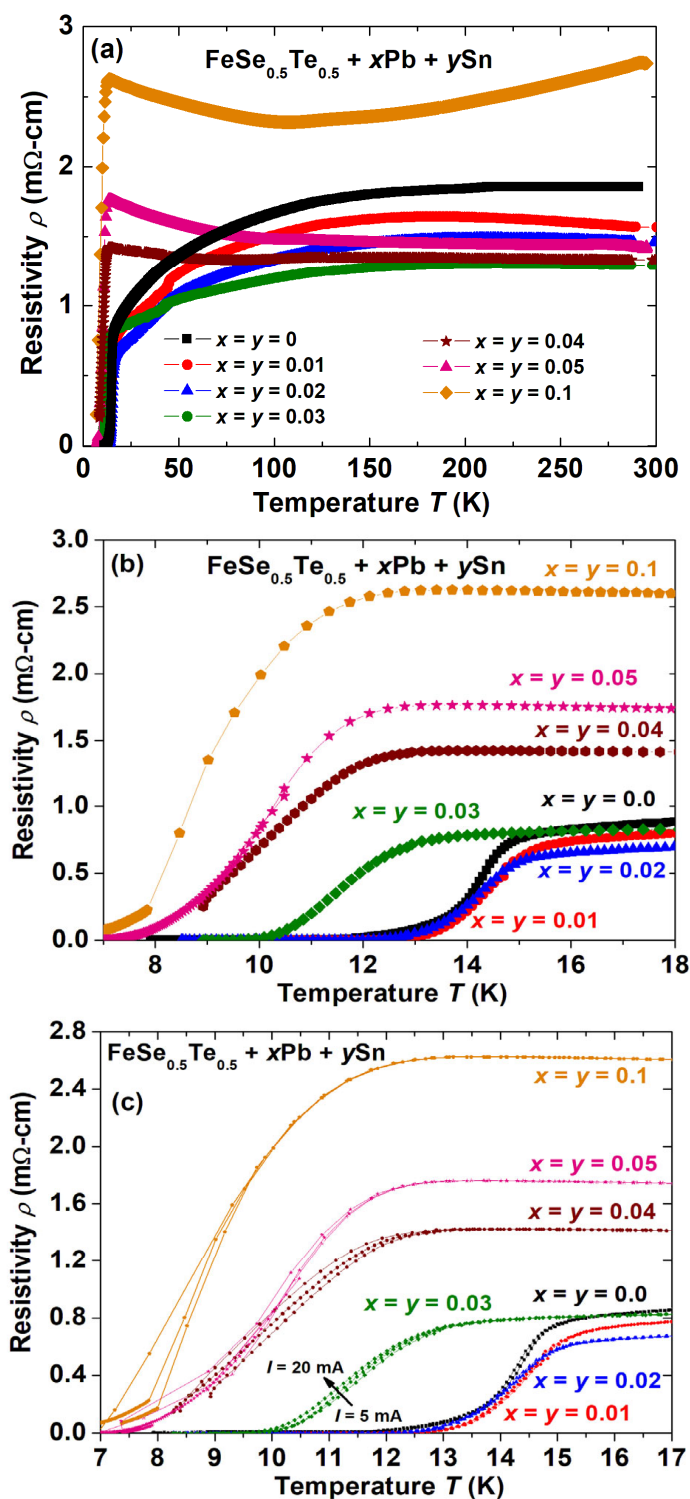


Figure 4. (a) The variation of resistivity (ρ) with respect to the temperature for all Pb- and Sn-added $\text{FeSe}_{0.5}\text{Te}_{0.5}$ bulks ($\text{FeSe}_{0.5}\text{Te}_{0.5} + x\text{Pb} + y\text{Sn}$ ($x = y = 0, 0.01, 0.02, 0.03, 0.04, 0.05,$ and 0.1)). (b) The resistivity behaviours with temperature for various samples in the low-temperature region (<20 K). (c) The low-temperature resistivity variation with temperature for $\text{FeSe}_{0.5}\text{Te}_{0.5} + x\text{Pb} + y\text{Sn}$ ($x = y = 0, 0.01, 0.02, 0.03, 0.04, 0.05,$ and 0.1) with respect to different currents $I = 5, 10, 20$ mA.

The low-temperature behaviour of the resistivity (ρ), as a function of temperature from 5 K to 18 K, is shown in Figure 4b, where each sample depicts a superconducting transition. The parent compound shows a transition temperature of around 14.8 K with a transition

width (ΔT) of 3.1 K. The samples with $x = y = 0.01$ and 0.02 have an enhanced transition temperature of 15.6 K and 15.4 K, respectively with a sharper superconducting transition. With further increases in Sn and Pb additions, the transition temperature is decreased with the broader transition width. Interestingly, the sample with $x = y = 0.03$ shows the onset transition of 12.8 K. With further increases in Sn and Pb additions, the onset T_c reduces very slowly but exhibits a relatively broad transition with a low T_c^{offset} . The onset T_c is observed around 12.1 K, 11.9 K, and 11.6 K for the samples with $x = y = 0.04$, $x = y = 0.05$, and $x = y = 0.1$, respectively.

More interestingly, their T_c^{offset} values differ significantly. According to reports, samples with 5% Pb addition show comparable T_c^{onset} values (13.8 K), which is around 1.1 K lower than the value for the Pb-free sample [38]. Chen et al. [39] reported that 5% Sn-added $\text{FeSe}_{0.5}\text{Te}_{0.5}$ ($x = 0, y = 0.05$) has $T_c^{\text{onset}} = 13.8$ K and $T_c^{\text{offset}} = 12$ K with respect to $T_c^{\text{onset}} = 13.5$ K and $T_c^{\text{offset}} = 9$ K of the parent compound which dramatically enhanced the zero resistivity temperature (T_c^{offset}) by 3 K accompanied by almost the same onset temperature of the superconducting transition (T_c^{onset}) [39]. Interestingly, a low amount of cometal Sn and Pb addition improved the onset transition temperature and also reduced the transition width, which works well accordingly to previous studies [38,39]. The sharper transition for the 1 and 2 wt% Sn- and Pb-added samples ($x = y = 0.01, 0.02$) suggests better grain connections and slightly higher Te/Se concentrations than the Sn- and Pb-free one ($x = y = 0$) which might be due to reducing the hexagonal phase, as discussed for XRD measurements. On the other hand, further increments of Sn and Pb addition exhibit the broadening of superconducting transition which might result due to the increased impurity phase ($\text{Pb}_{0.85}\text{Sn}_{0.15}\text{Te}_{0.85}\text{Se}_{0.15}$) and the decreased superconducting phase. The slight decrease in the lattice parameters with Sn and Pb addition, as mentioned in Table 1, suggests that there is a lower Se/Te concentration in the $\text{FeSe}_{0.5}\text{Te}_{0.5}$ composition, which is also supported by EDAX measurements (Table 2). This could be a possible reason for the reduced transition temperature T_c at high Pb and Sn additions. The reported study based on Li-doped $\text{FeSe}_{0.5}\text{Te}_{0.5}$ [37] has confirmed that the doping element Li entered the crystal structure of Fe(Se,Te) and enhanced the superconducting transition by 1–1.5 K for 1 wt% doping without affecting the T_c^{offset} . In contrast to these earlier findings, adding 5% Sn to $\text{FeSe}_{0.5}\text{Te}_{0.5}$ can significantly raise T_c^{offset} by 3 K without affecting T_c^{onset} while not altering the crystal structure of the compound. The magnetic elements such as Co and Ni at Fe sites reduce the superconducting properties of $\text{FeSe}_{0.5}\text{Te}_{0.5}$ [41]. Our current results show the enhancement of T_c^{onset} by ~ 1 K and also slightly improved T_c^{offset} by a very small amount of Sn- and Pb-added samples without entering the crystal structure of $\text{FeSe}_{0.5}\text{Te}_{0.5}$ which implies that a small amount of Sn and Pb ($x = y \leq 0.02$) seems to be the most promising additive among metals to further improve the superconductivity in the 11-type FBSs.

The offset transition temperature (T_c^{offset}) generally relates to the grain connections, i.e., the intergrain effect, whereas the onset transition temperature (T_c^{onset}) represents the specific grain effect, i.e., the intragrain effect [50,51]. These effects can be understood by the resistivity measurements under different applied currents. To understand the grain connectivity behaviours of our bulk samples, we have depicted the low-temperature resistivity behaviours of various bulk samples with three different currents, $I = 5, 10$, and 20 mA, in Figure 4c. The bulk samples with $x = y = 0.01$ and 0.02 have almost no transition broadening with various currents and also a sharper transition compared to that of the parent compound ($x = y = 0$). The transition broadening is increased for higher Pb and Sn additions ($x = y \geq 0.02$), and the offset transition is more sensitive with the applied currents, as shown in Figure 4c which could be due to the enhanced impurity phases as observed from XRD patterns. It clearly suggests that a low amount of cometal ($x = y = 0.01$ and 0.02)-added samples have a better intergrain effect than that of the parent compound. These outcomes support the analysis of microstructural studies, as discussed above. A previous study shows that 5 wt% Pb-added $\text{FeSe}_{0.5}\text{Te}_{0.5}$ has almost the same broadening with applied current as that of the parent compound but has a sharper transition. However, higher Pb additions reduce the grain connections due to the enhancement of the impurity

phase. Compared to our results with only Pb-added samples, a low amount of cometal additions to $\text{FeSe}_{0.5}\text{Te}_{0.5}$ has almost no broadening of the transition with respect to the applied current, which suggests better grain connectivity. These results well agree with microstructural and XRD analysis.

Magnetic moment hysteresis loops $M(H)$ at a constant temperature of 7 K for $x = y = 0$, $x = 0.05$, $y = 0$; $x = y = 0.01$, 0.02, and 0.03 were measured with the rectangular-shaped sample in order to determine the persistent critical current density J_c . The measured magnetic loops $M(H)$ for these samples were observed under ferromagnetic effects, which is similar to previous reports based on FeSe samples [29,38,52]. The inset of Figure 5a shows the $M(H)$ loop for Pb- and Sn-added samples with $x = y = 0.02$, which is depicted after the subtraction of the normal state magnetisation, i.e., the $M(H)$ loop at 22 K. Similar magnetisation loops, with larger backgrounds, however, were obtained for a sample with high Pb and Sn additions.

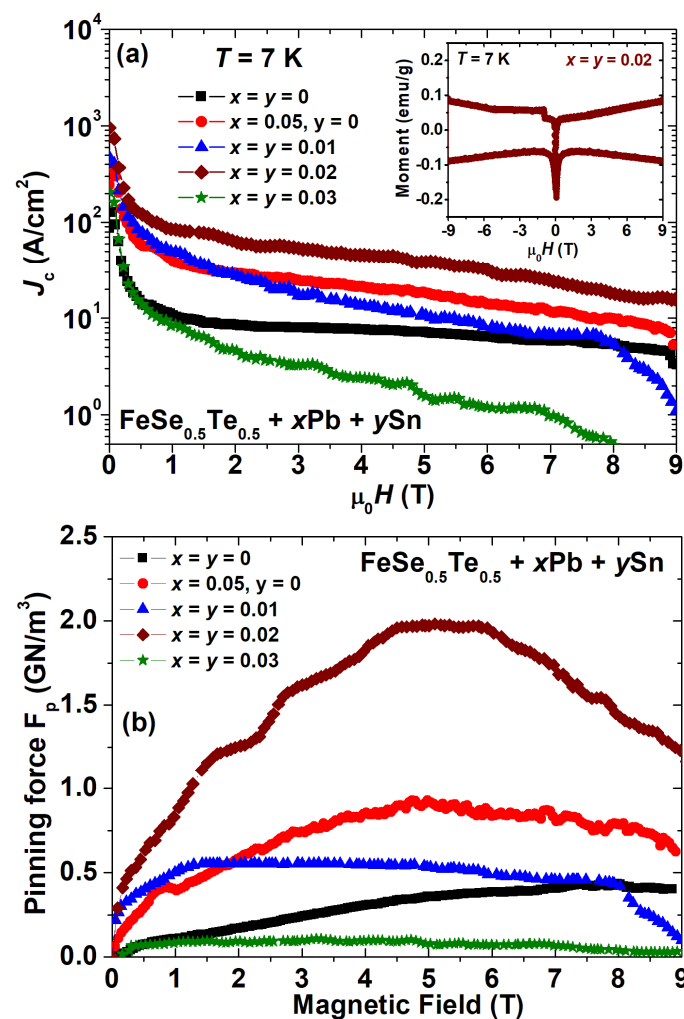


Figure 5. (a) The magnetic field (H) dependence of critical current density (J_c) for $\text{FeSe}_{0.5}\text{Te}_{0.5} + x\text{Pb} + y\text{Sn}$ ($x = y = 0, 0.01, 0.02, 0.03$, and $x = 0.05, y = 0$) samples with respect to the parent compound $\text{FeSe}_{0.5}\text{Te}_{0.5}$ at a temperature of 7 K. The inset figure shows the magnetic hysteresis loop $M(H)$ at 7 K for $x = y = 0.02$ after the subtraction of the normal state background. (b) The variation of pinning force F_p with respect to the applied magnetic field at 7 K for various bulk $\text{FeSe}_{0.5}\text{Te}_{0.5} + x\text{Pb} + y\text{Sn}$ ($x = y = 0, 0.01, 0.02, 0.03$, and $x = 0.05, y = 0$) samples.

These hysteresis loops allow us to estimate the critical current density, which is an important parameter for practical applications. The Bean critical state model [53] was applied to obtain the critical state densities from the magnetisation loops. The calcula-

tion of the critical current density J_c for our samples was performed using the formula $J_c = 20\Delta m/Va(1-a/3b)$ [53], where Δm is the hysteresis loop width, V is the volume of the sample, and a and b are the lengths of the shorter and longer edge, respectively. Figure 5a depicts the magnetic field dependence of the critical current density (J_c) up to 9 T at 7 K for the parent compound with various Pb- and Sn-added samples. J_c values of the parent compounds were enhanced by adding 5 wt% Pb to $\text{FeSe}_{0.5}\text{Te}_{0.5}$ ($x = 0.05, y = 0$), whereas, with the addition of Sn and Pb, i.e., $x = y = 0.02$, the J_c values are further enhanced in the whole magnetic field range up to 9 T. Interestingly, the calculated J_c of samples $x = y = 0.01$ and 0.02 has field dependence almost similar to that of Pb-added samples ($x = 0.05, y = 0$) and enhanced one order of magnitude of the J_c values compared to the parent compound. This improvement in J_c values suggests that cometal inclusion is capable of providing effective flux-pinning centres. It could be possible due to the increased density and improved grain connections caused by the addition of a small amount of Sn and Pb, which are clearly observed in the microstructural analysis and resistivity studies. In pure bulk MgB_2 polycrystalline samples, the same observation was observed [54], where Ag nanoparticle addition enhances the J_c value due to extra pinning centres. One should note an important point that the 5% Pb-added sample ($x = 0.05, y = 0$) has almost the same J_c values [38] and similar behaviour as that of 1% Sn- and Pb-added samples ($x = y = 0.01$). It clearly suggests that Sn can be the most effective metal to enhance the J_c value for $\text{FeSe}_{0.5}\text{Te}_{0.5}$ samples, which is comparable to the reported elevation of J_c values for Sn-added $\text{SmFeAs}(\text{O},\text{F})$ [50] where Sn additions also work more effectively to improve the intergranular current than that of other metal additions [30].

To understand the pinning behaviours of these samples, the magnetic field dependence of the vortex pinning force density, F_p , has been calculated by $F_p = \mu_0 H \times J_c$ [55] with the obtained J_c values at 7 K which are depicted in Figure 5b for various samples. The F_p curves of the parent compound increase with magnetic fields and reach a maximum around 8–9 T, whereas 1 wt% Pb and Sn additions show a maximum of F_p for low magnetic fields, and then they decrease very slowly with the applied fields. Further Sn and Pb additions enhance F_p values in the whole measured fields and shift the maximum of F_p to the higher magnetic field as similar to 5 wt% Pb-added samples ($x = 0.05, y = 0$). The samples with $x = y = 0.03$ showed similar behaviours to 1 wt% Pb- and Sn-added $\text{FeSe}_{0.5}\text{Te}_{0.5}$ but with lower values of F_p compared to all other samples depicted in Figure 5b. This is unusual behaviour, most likely caused by cometal addition, that warrants further investigation to understand how cometal additions can influence the vortex pinning mechanisms in $\text{FeSe}_{0.5}\text{Te}_{0.5}$ compounds. The F_p values are enhanced up to the intermediate field (~5–6 T) range for the small amount of Pb- and Sn-added $\text{FeSe}_{0.5}\text{Te}_{0.5}$ ($x = y \leq 0.02$) compared to that of the parent compound ($x = y = 0$) which is in nice agreement with the J_c enhancement as depicted in Figure 5a. Briefly, 5 wt% Pb-added samples ($x = 0.05, y = 0$) also enhanced the F_p values, which are similar to the previous report [38] and higher than those of 1 wt% Pb- and Sn-added samples and their parent compounds. Furthermore, the obtained F_p values of the parent compounds are almost the same as those reported (0.1–1 GN/m³) in previous studies [52,56] based on polycrystalline $\text{Fe}(\text{Se}, \text{Te})$ samples. The F_p behaviour leads us to the conclusion that improving the appropriate pinning centres is a reason for the enhancement of the critical current behaviours. There are also reports of similar results for Ag-added MgB_2 [54] and Sn-added alternative FBS bulk samples [50]. High-pressure techniques such as high-pressure growth and high-pressure sintering can be used to further improve the J_c and F_p of these samples [2,56].

To summarise the main findings of our study, the variation of transition temperature T_c^{onset} , the transition width (ΔT), the room temperature resistivity ($\rho_{300\text{K}}$), the RRR ($\rho_{300\text{K}}/\rho_{20\text{K}}$), and the critical current density (J_c) for 0 T and 5 T at 7 K with weight concentrations of Pb- and Sn-added samples (x, y) are shown in Figure 6a–e. The T_c^{onset} is enhanced by ~1 K for 1 and 2 wt% Pb- and Sn-added samples. With further increases in the weight of these concentrations, the T_c^{onset} value starts to decrease (Figure 6a). The value of transition width $\Delta T (= T_c^{\text{onset}} - T_c^{\text{offset}})$ also reduces with a small amount of Sn and Pb

addition and reaches a minimum value for 2% weight Pb and Sn addition; i.e., it has a sharp transition with respect to other samples as depicted in Figure 6b. This is a clear indication of higher homogeneity, better grain connectivity, and phase purity of this sample compared to other samples. On the other hand, the broadening of the transition, i.e., the transition width ΔT starts to enhance with further increases in Pb and Sn additions and becomes almost saturated for $x = y \geq 0.04$. The addition of Pb and Sn also enhanced the metallic nature of the $\text{FeSe}_{0.5}\text{Te}_{0.5}$ sample at room temperature; i.e., the resistivity $\rho_{300\text{K}}$ decreased for a low amount of metal additions, as shown in Figure 6c, and $\rho_{300\text{K}}$ reached minimum values for 3 and 4% weight Sn- and Pb-added samples. With further enhancements of Pb and Sn, $\rho_{300\text{K}}$ started to increase, which is due to the enhancement of the impurity phases as discussed above. We also calculated and plotted the residual resistivity ratio RRR value for all samples, as depicted in Figure 6d. The maximum RRR is observed for the samples with $x = y = 0.02$, and after that, RRR started to decrease with further increases in Pb and Sn additions.

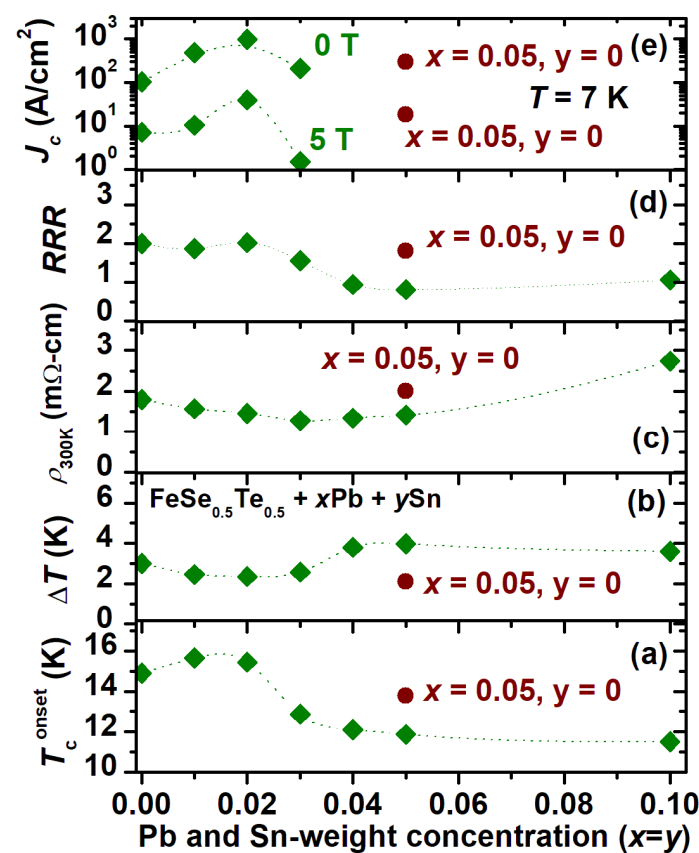


Figure 6. The variation of (a) transition temperature (T_c), (b) transition width (ΔT), (c) room temperature resistivity $\rho_{300\text{K}}$, (d) residual resistivity ratio RRR ($\rho_{300\text{K}}/\rho_{20\text{K}}$) and (e) the critical current density J_c for 0 T and 5 T at 7 K with respect to weight% of Pb and Sn addition for parent $\text{FeSe}_{0.5}\text{Te}_{0.5}$, i.e., $\text{FeSe}_{0.5}\text{Te}_{0.5} + x\text{Pb} + y\text{Sn}$ ($x = y = 0, 0.01, 0.02, 0.03, 0.04, 0.05$, and 0.1) and also only Pb-added $\text{FeSe}_{0.5}\text{Te}_{0.5}$ ($x = 0.05, y = 0$).

The maximum of RRR and the minimum of ΔT are other transport signatures of the high quality of the polycrystalline samples with $x = y = 0.02$. The onset T_c was reduced, and the transition width, ΔT , and $\rho_{300\text{K}}$ were enhanced with increasing Pb and Sn additions. It is worth noting that the RRR for our best samples was 2.2, which is higher than the reported value (1.3) for the 5 and 10% Sn-added $\text{FeSe}_{0.5}\text{Te}_{0.5}$ samples [39] and also better than the reported (1.8) for the Pb-added $\text{FeSe}_{0.5}\text{Te}_{0.5}$ samples [38]. A very small amount of Sn and Pb additions improved the overall RRR of the parent compound, as similar to those reported for Ag, Sn, and Pb additions [32,38,39]. Meanwhile, 1 and 2 wt% Sn- and Pb-added samples

show a ~ 1 K higher transition and a comparatively sharper transition width with T_c of 15.6 K and a T_c^{offset} of 13.2 K. The transition width of 2.4 K suggests a sharper transition than for the pure sample. In Figure 5e, we plot the J_c values at 0 T and 5 T for various Pb- and Sn-added samples with parent and only 5% Pb-added samples. It clearly indicates that a very small amount of the addition of Sn and Pb creates effective pinning centres and, in consequence, improves the critical current density by an order of magnitude with respect to the parent compound and also only Pb-added samples. This analysis suggests that a small amount of cometal addition improves both the superconducting properties and also the granular behaviour.

Disorder can significantly enhance superconductivity and has been utilised as an effective method to explore superconducting order [57–59]. Strong disorder, on the other hand, increases phase fluctuations, which lowers the superfluid density and suppresses superconductivity globally [59,60]. As the disorder strength is varied, an optimal degree of inhomogeneity can be reached which enhances the superconducting properties and the transition temperature T_c to reach the maximum value. Outside that region, strong disorder reduces superconductivity and can even cause a superconductor–insulator transition [61], as observed in conventional superconductors, which are usually believed to be insensitive to small concentrations of random nonmagnetic impurities [62]. On this basis, here, we can explain the enhancement of the superconducting properties of $\text{FeSe}_{0.5}\text{Te}_{0.5}$ with the correlation effect in the disorder which is generated by nonmagnetic cometal addition. A large amount of Pb and Sn addition generally creates strong disorder due to a large amount of impurity phase, as discussed above, and its behaviour shifts to the superconductor–insulation transition which is clearly observed through the resistivity measurements for high-Pb- and Sn-added $\text{FeSe}_{0.5}\text{Te}_{0.5}$ samples ($x = y \geq 0.04$) (Figure 4a). A very small amount of cometal addition such as (below $x = y = 0.01$) does not affect the superconducting properties, as observed from Figure 6 with the dotted line, and more than 3 wt% cometal addition induces strong disorder which enhances rapidly with further Pb and Sn additions. On these analyses, we can conclude that 1 to 2 wt% cometal addition is the optimum region where the disorder strength improves the superconducting properties of the $\text{FeSe}_{0.5}\text{Te}_{0.5}$ bulk. Hence, it seems that the enhanced superconductivity of these materials is related to the effects of the disorder correlations as is well-reported for other superconductors [59].

4. Conclusions

We studied the cometal addition effect on the superconducting properties of $\text{FeSe}_{0.5}\text{Te}_{0.5}$ through various characterisations. Structural analysis of the prepared $\text{FeSe}_{0.5}\text{Te}_{0.5}$ samples with Pb and Sn additions showed that these metals do not enter in the superconducting tetragonal structure of $\text{FeSe}_{0.5}\text{Te}_{0.5}$ and lattice parameters seem to be unaffected by these additions. A large amount of Sn and Pb additions ($x = y > 0.02$) enhanced the impurity phases and introduced inhomogeneities into the samples, resulting in a change in the Fe/Se/Te ratio from the stoichiometric $\text{FeSe}_{0.5}\text{Te}_{0.5}$ composition. However, very low amounts of Pb and Sn additions were effective in enhancing the transition temperature of T_c and J_c in the measured magnetic field (up to 9 T) due to the improved grain connections as well as the presence of additional pinning centres. Microstructural analysis shows disc-shaped superconducting grains, and at high Pb and Sn additions, the intergrain connections were reduced compared to low amounts of Sn- and Pb-added samples and their parent compounds. A cometal addition effect on iron-based superconductors has been studied for the first time, confirming that cometal additions can be a potential way to enhance superconducting properties with the improvement of sample qualities. We believe that this method will enable the further exploration of Fe(Se, Te) and other FBS materials to achieve additional improvements in their superconducting properties and the development of their magnetic applications, especially with respect to superconducting wires and tapes.

Author Contributions: Conceptualisation, Supervision and Formal analysis, S.J.S. and A.W.; methodology, S.J.S.; XRD data analysis, S.J.S. and R.D.; Magnetic data collection, T.Z., M.M. and M.A.; Transport and SEM data collections, M.M., M.A. and T.C.; investigation and writing—original draft preparation, S.J.S. and M.M.; writing—review and editing, S.J.S. and A.W.; Comments and Suggestions, M.M., M.A., T.Z., T.C., A.M., R.D. and A.W. All authors have read and agreed to the published version of the manuscript.

Funding: This research was funded by National Science Centre (NCN), Poland, grant number “2021/42/E/ST5/00262” (SONATA-BIS 11). S.J.S. acknowledges financial support from National Science Centre (NCN), Poland through research Project number: 2021/42/E/ST5/00262.

Institutional Review Board Statement: Not applicable.

Informed Consent Statement: Not applicable.

Data Availability Statement: Data are available upon request to the corresponding author.

Conflicts of Interest: The authors declare no conflict of interest.

References

1. Si, Q.; Yu, R.; Abrahams, E. High-temperature superconductivity in iron pnictides and chalcogenides. *Nat. Rev. Mater.* **2016**, *1*, 16017. [[CrossRef](#)]
2. Singh, S.J.; Sturza, M. Bulk and Single Crystal Growth Progress of Iron-Based Superconductors (FBS): 1111 and 1144. *Crystals* **2022**, *12*, 20. [[CrossRef](#)]
3. Kamihara, Y.; Watanabe, T.; Hirano, M.; Hosono, H. Iron-Based Layered Superconductor La[O_{1-x}F_x]FeAs (x = 0.05 – 0.12) with T_c = 26 K. *J. Am. Chem. Soc.* **2008**, *130*, 3296. [[CrossRef](#)] [[PubMed](#)]
4. Singh, S.J.; Morawska, A. New Potential Family of Iron Based Superconductors towards practical application: CaKFe₄As₄. In *High-Tc Superconducting Technology: Towards Sustainable Development Goals*; Jenny Stanford Publishing: New York, NY, USA, 2021; pp. 283–314. [[CrossRef](#)]
5. Singh, S.J.; Mele, P. Future Potential of New High T_c Iron-Based Superconductors. In *Superconductivity: From Materials Science to Practical Applications*; Springer: Berlin/Heidelberg, Germany, 2020; pp. 243–268. [[CrossRef](#)]
6. Hosono, H.; Yamamoto, A.; Hiramatsu, H.; Ma, Y. Recent advances in iron-based superconductors toward applications. *Mater. Today* **2018**, *21*, 278–302. [[CrossRef](#)]
7. Hsu, F.C.; Luo, J.Y.; Yeh, K.W.; Chen, T.K.; Huang, T.W.; Wu, P.M.; Lee, Y.C.; Huang, Y.L.; Chu, Y.Y.; Yan, D.C.; et al. Superconductivity in the PbO-type structure α -FeSe. *Proc. Natl. Acad. Sci. USA* **2008**, *105*, 14262. [[CrossRef](#)] [[PubMed](#)]
8. Mizuguchi, Y.; Tomioka, F.; Tsuda, S.; Yamaguchi, T.; Takano, Y. Substitution Effects on FeSe Superconductor. *J. Phys. Soc. Jpn.* **2009**, *78*, 074712. [[CrossRef](#)]
9. Shibauchi, T.; Hanaguri, T.; Matsuda, Y. Exotic Superconducting States in FeSe-based Materials. *J. Phys. Soc. Jpn.* **2020**, *89*, 102002. [[CrossRef](#)]
10. Dong, X.; Zhou, F.; Zhao, Z. Electronic and Superconducting Properties of Some FeSe-Based Single Crystals and Films Grown Hydrothermally. *Front. Phys.* **2020**, *586182*, 8. [[CrossRef](#)]
11. Margadonna, S.; Takabayashi, Y.; Ohishi, Y.; Mizuguchi, Y.; Takano, Y.; Kagayama, T.; Nakagawa, T.; Takata, M.; Prassides, K. Pressure evolution of the low-temperature crystal structure and bonding of the superconductor FeSe. *Phys. Rev. B* **2009**, *80*, 064506. [[CrossRef](#)]
12. Guo, J.; Jin, S.; Wang, G.; Wang, S.; Zhu, K.; Zhou, T.; He, M.; Chen, X. Superconductivity in the iron selenide K_xFe₂Se₂ (0 ≤ x ≤ 1.0). *Phys. Rev. B* **2010**, *82*, 180520R. [[CrossRef](#)]
13. Fang, M.H.; Wang, H.D.; Dong, C.H.; Li, Z.J.; Feng, C.M.; Chen, J.; Yuan, H.Q. Fe-based superconductivity with T_c = 31 K bordering an antiferromagnetic insulator in (Tl,K)FexSe₂. *Europhys. Lett.* **2011**, *94*, 27009. [[CrossRef](#)]
14. Lu, X.F.; Wang, N.Z.; Wu, H.; Wu, Y.P.; Zhao, D.; Zeng, X.Z.; Luo, X.G.; Wu, T.; Bao, W.; Zhang, G.H.; et al. Coexistence of superconductivity and antiferromagnetism in (Li_{0.8}Fe_{0.2})OHFeSe. *Nat. Mater.* **2014**, *14*, 325. [[CrossRef](#)]
15. Wang, Q.-Y.; Li, Z.; Zhang, W.-H.; Zhang, Z.-C.; Zhang, J.-S.; Li, W.; Ding, H.; Ou, Y.-B.; Deng, P.; Chang, K.; et al. Interface-induced high-temperature superconductivity in single unit-cell FeSe films on SrTiO₃. *Chin. Phys. Lett.* **2012**, *29*, 037402. [[CrossRef](#)]
16. He, S.; He, J.; Zhang, W.; Zhao, L.; Liu, D.; Liu, X.; Mou, D.; Ou, Y.B.; Wang, Q.Y.; Li, Z.; et al. Phase diagram and electronic indication of high-temperature superconductivity at 65 K in single-layer FeSe films. *Nat. Mater.* **2013**, *12*, 605. [[CrossRef](#)]
17. William, A.J.; McQueen, T.M.; Ksenofontov, V.; Felser, C.; Cava, R.J. The metal-insulator transition in Fe_(1.01-x)Cu_(x)Se. *J. Phys. Condens. Matter* **2009**, *21*, 305701. [[CrossRef](#)]
18. Zajicek, Z.; Singh, S.J.; Jones, H.; Reiss, P.; Bristow, M.; Martin, A.; Gower, A.; McCollam, A.; Coldea, A.I. The drastic effect of the impurity scattering on the electronic and superconducting properties of Cu-doped FeSe. *Phys. Rev. B* **2022**, *105*, 115130. [[CrossRef](#)]
19. Shipra, R.; Takeya, H.; Hirata, K.; Sundaresan, A. Effects of Ni and Co doping on the physical properties of tetragonal FeSe_{0.5}Te_{0.5} superconductor. *Phys. C Supercond.* **2010**, *470*, 528. [[CrossRef](#)]

20. Yadav, A.K.; Thakur, A.D.; Tomy, C.V. Enhanced superconducting properties in FeCr_xS. *Solid State Commun.* **2011**, *151*, 557. [[CrossRef](#)]
21. Ma, Q.; Gao, Q.; Shan, W.; Li, X.; Li, H.; Ma, Z. The superconductivity and transport properties in FeTe with S addition. *Vacuum* **2022**, *195*, 110661. [[CrossRef](#)]
22. Coldea, A. Electronic Nematic States Tuned by Isoelectronic Substitution in Bulk FeSe_{1-x}S_x. *Front. Phys.* **2021**, *8*, 594500. [[CrossRef](#)]
23. Viennois, R.; Giannini, E.; van der Marel, D.; Černý, R. Effect of Fe excess on structural, magnetic and superconducting properties of single-crystalline Fe_{1+x}Te_{1-y}Se_y. *J. Solid State Chem.* **2010**, *183*, 769. [[CrossRef](#)]
24. Sales, B.C.; Sefat, A.S.; McGuire, M.A.; Jin, R.Y.; Mandrus, D.; Mozharivskyj, Y. Bulk superconductivity at 14 K in single crystals of Fe_{1+y}Te_xSe_{1-x}. *Phys. Rev. B* **2009**, *79*, 094521. [[CrossRef](#)]
25. Tsurkan, V.; Deisenhofer, J.; Günther, A.; Kant, C.; von Nidda, H.-A.K.; Schrettle, F.; Loidl, A. Physical properties of FeSe_{0.5}Te_{0.5} single crystals grown under different conditions. *Eur. Phys. J. B* **2011**, *79*, 289–299. [[CrossRef](#)]
26. Her, J.L.; Kohama, Y.; Matsuda, Y.H.; Kindo, K.; Yang, W.-H.; Chareev, D.A.; Mitrofanova, E.S.; Volkova, O.S.; Vasiliev, A.N.; Lin, J.-Y. Anisotropy in the upper critical field of FeSe and FeSe_{0.33}Te_{0.67} single crystals. *Supercond. Sci. Technol.* **2015**, *28*, 045013. [[CrossRef](#)]
27. Takano, Y.; Mizuguchi, Y. Review of Fe Chalcogenides as the Simplest Fe-Based Superconductor. *J. Phys. Soc. Jpn.* **2010**, *79*, 102001.
28. Okamoto, H. The Fe–Se (iron-selenium) system. *J. Phase Equilibria* **1991**, *12*, 383. [[CrossRef](#)]
29. Nouailhetas, Q.; Koblishka-Veneva, A.; Koblishka, M.R.; Naik, S.P.; Schäfer, F.; Ogino, H.; Motz, C.; Berger, K.; Douine, B.; Slimani, Y.; et al. Magnetic phases in superconducting, polycrystalline bulk FeSe samples. *AIP Adv.* **2021**, *11*, 015230. [[CrossRef](#)]
30. Ma, Y. Progress in wire fabrication of iron-based superconductors. *Supercond. Sci. Technol.* **2012**, *25*, 113001. [[CrossRef](#)]
31. Feldmann, D.M.; Holesinger, T.G.; Feenstra, R.; Larbalestier, D.C. A Review of the Influence of Grain Boundary Geometry on the Electromagnetic Properties of Polycrystalline YBa₂Cu₃O_{7-x} Films. *J. Am. Ceram. Soc.* **2008**, *91*, 1869. [[CrossRef](#)]
32. Koblishka, M.R.; Slimani, Y.; Koblishka-Veneva, A.; Karwoth, T.; Zeng, X.; Hannachi, E.; Murakami, M. Excess Conductivity Analysis of Polycrystalline FeSe Samples with the Addition of Ag. *Materials* **2020**, *13*, 5018. [[CrossRef](#)]
33. Ma, Y.; Zhang, X. Significantly enhanced critical current densities in MgB₂ tapes made by a scaleable nanocarbon addition route. *Appl. Phys. Lett.* **2006**, *88*, 072502. [[CrossRef](#)]
34. Lee, D.F.; Chaud, X.; Salama, K. Transport current density in bulk oriented-grained YBa₂Cu₃O_x/silver composites. *Phys. C* **1991**, *181*, 81–87. [[CrossRef](#)]
35. Migita, M.; Takikawa, Y.; Sugai, K.; Takeda, M.; Uehara, M.; Kuramoto, T.; Takano, Y.; Mizuguchi, Y.; Kimishima, Y. Substitution effects of Ag into FeSe_{0.5}Te_{0.5} superconductor. *Phys. C Supercond.* **2013**, *484*, 66. [[CrossRef](#)]
36. Kumar, A.; Tandon, R.P.; Awana, V.P.S. Effect of 3d metal (Co and Ni) doping on the superconductivity of FeSe_{0.5}Te_{0.5}. *IEEE Trans. Magn.* **2012**, *48*, 4239. [[CrossRef](#)]
37. Yang, C.M.; Chen, P.W.; Chen, I.G.; Qi, X.D.; Yan, D.C.; Wu, M.K. Enhancement of superconductivity in FeSe_{1-x}Te_x by Li doping. *Supercond. Sci. Technol.* **2012**, *25*, 095010. [[CrossRef](#)]
38. Singh, S.J.; Diduszko, R.; Iwanowski, P.; Cetner, T.; Wisniewski, A.; Morawski, A. Effect of Pb addition on microstructure, transport properties, and the critical current density in a polycrystalline FeSe_{0.5}Te_{0.5}. *Appl. Phys. A* **2022**, *128*, 476. [[CrossRef](#)]
39. Chen, N.; Liu, Y.; Ma, Z.; Li, H.; Al Hossain, M.S. Enhancement of superconductivity in the sintered FeSe_{0.5}Te_{0.5} bulks. *J. Alloy. Compd.* **2015**, *633*, 233–236. [[CrossRef](#)]
40. Roisnel, T.; Rodríguez-Carvajal, J. Winplotr: A windowtool for powder diffraction pattern analysis. *Mater. Sci. Forum* **2001**, *118*, 378. [[CrossRef](#)]
41. Cieplak, M.Z.; Bezusyy, V.L. Transition metal doping of FeSeTe: What can we learn from transport properties. *Philos. Mag. A* **2015**, *95*, 480–492. [[CrossRef](#)]
42. Kametani, F.; Polyanskii, A.A.; Yamamoto, A.; Jiang, J.; Hellstrom, E.E.; Gurevich, A.; Larbalestier, D.C.; Ren, Z.A.; Yang, J.; Dong, X.L. Combined microstructural and magneto optical study of current flow in Nd and Sm Fe-oxypnictides. *Supercond. Sci. Technol.* **2009**, *22*, 015010. [[CrossRef](#)]
43. Singh, S.J.; Beck, R.; Wurmehl, S.; Hess, C.; Büchner, B. Granular behavior observed in the polycrystalline superconducting LiFeAs. *Supercond. Sci. Technol.* **2015**, *28*, 025006. [[CrossRef](#)]
44. Schuster, W.; MiMer, H.; Komarek, K.L. Transition metal–chalcogen systems VII: The iron–selenium phase diagram. *Monats. Chem.* **1979**, *110*, 1153–1170. [[CrossRef](#)]
45. Lin, H.; Yao, C.; Zhang, X.; Zhang, H.; Zhang, Q.; Wang, D.; Dong, C.; Ma, Y. Effect of metal (Zn/In/Pb) additions on the microstructures and superconducting properties of Sr_{1-x}K_xFe₂As₂ tapes. *Scr. Mater.* **2016**, *112*, 128. [[CrossRef](#)]
46. Singh, S.J.; Shimoyama, J.-I.; Yamamoto, A.; Ogino, H.; Kishio, K. Significant enhancement of the intergrain coupling in lightly F-doped SmFeAsO superconductors. *Supercond. Sci. Technol.* **2013**, *26*, 065006. [[CrossRef](#)]
47. Yeh, K.-W.; Huang, T.-W.; Huang, Y.-L.; Chen, T.-K.; Hsu, F.-C.; Wu, P.M.; Lee, Y.-C.; Chu, Y.-Y.; Chen, C.-L.; Luo, J.-Y.; et al. Tellurium substitution effect on superconductivity of the α-phase iron selenide. *Europhys. Lett.* **2008**, *84*, 37002. [[CrossRef](#)]
48. Yuan, R.H.; Kong, W.D.; Yan, L.; Ding, H.; Wang, N.L. In-plane optical spectroscopy study on FeSe epitaxial thin film grown on SrTiO₃ substrate. *Phys. Rev. B* **2013**, *87*, 144517. [[CrossRef](#)]

49. Gebre, T.; Li, G.; Whalen, J.B.; Conner, B.S.; Zhou, H.D.; Grissonnanche, G.; Kostov, M.K.; Gurevich, A.; Siegrist, T.; Balicas, L. Disorder-dependent superconducting phase-diagram at high magnetic fields in $\text{Fe}_{1+y}\text{Se}_x\text{Te}_{1-x}$. *Phys. Rev. B* **2011**, *84*, 174517. [[CrossRef](#)]
50. Singh, S.J.; Shimoyama, J.-I.; Ogino, H.; Yamamoto, A.; Kishio, K. Enhancement of intergranular current density of Sm-based oxypnictide superconductors with Sn addition. *Supercond. Sci. Technol.* **2014**, *27*, 085010. [[CrossRef](#)]
51. Singh, S.J.; Ogino, H.; Shimoyama, J.-I.; Kishio, K. Weak-link behaviour observed in iron-based superconductors with thick perovskite-type blocking layers. *Supercond. Sci. Technol.* **2013**, *26*, 105020. [[CrossRef](#)]
52. Galluzzi, A.; Buchkov, K.; Tomov, V.; Nazarova, E.; Leo, A.; Grimaldi, G.; Polichetti, M. High Pinning Force Values of a Fe(Se, Te) Single Crystal Presenting a Second Magnetization Peak Phenomenon. *Materials* **2021**, *14*, 5214. [[CrossRef](#)]
53. Bean, C.P. Magnetization of high-field superconductors. *Rev. Mod. Phys.* **1985**, *36*, 31. [[CrossRef](#)]
54. Shekhar, C.; Giri, R.; Tiwari, R.S.; Srivastava, O.N.; Malik, S.K. High critical current density and improved flux pinning in bulk MgB_2 synthesized by Ag addition. *J. Appl. Phys.* **2007**, *101*, 043906. [[CrossRef](#)]
55. Dew-Hughes, D. Flux pinning mechanisms in type II superconductors. *Philos. Mag.* **1974**, *30*, 293–305. [[CrossRef](#)]
56. Zignani, C.F.; De Marzi, G.; Corato, V.; Mancini, A.; Vannozzi, A.; Rufoloni, A.; Leo, A.; Guarino, A.; Galluzzi, A.; Nigro, A.; et al. Improvements of high-field pinning properties of polycrystalline Fe(Se, Te) material by heat treatments. *J. Mater. Sci.* **2019**, *54*, 5092–5100. [[CrossRef](#)]
57. Römer, A.T.; Hirschfeld, P.J.; Andersen, B.M. Raising the Critical Temperature by Disorder in Unconventional Superconductors Mediated by Spin Fluctuations. *Phys. Rev. Lett.* **2018**, *121*, 027002. [[CrossRef](#)]
58. Mayoh, J.; Garcia-Garcia, A.M. Strong enhancement of bulk superconductivity by engineered nanogranularity. *Phys. Rev. B* **2014**, *90*, 134513. [[CrossRef](#)]
59. Neverov, V.D.; Lukyanov, A.E.; Krasavin, A.V.; Vagov, A.; Croitoru, M.D. Correlated disorder as a way towards robust superconductivity. *Commun. Phys.* **2022**, *5*, 177. [[CrossRef](#)]
60. Croitoru, M.D.; Shanenko, A.A.; Vagov, A.; Vasenko, A.S.; Milosevic, M.V.; Axt, V.M.; Peeters, F.M. Influence of Disorder on Superconducting Correlations in Nanoparticles. *J. Supercond. Nov. Magn.* **2016**, *29*, 605. [[CrossRef](#)]
61. Feigel'man, M.V.; Ioffe, L.B.; Kravtsov, V.E.; Yuzbashyan, E.A. Eigenfunction Fractality and Pseudogap State near the Superconductor-Insulator Transition. *Phys. Rev. Lett.* **2007**, *98*, 027001. [[CrossRef](#)] [[PubMed](#)]
62. Abrikosov, A.; Gor'kov, L. Contribution of the theory of superconducting alloys with paramagnetic impurities. *Sov. Phys. JETP* **1961**, *12*, 1243.

Disclaimer/Publisher's Note: The statements, opinions and data contained in all publications are solely those of the individual author(s) and contributor(s) and not of MDPI and/or the editor(s). MDPI and/or the editor(s) disclaim responsibility for any injury to people or property resulting from any ideas, methods, instructions or products referred to in the content.